# A Design Strategy for a 6:1 Supersonic Mixed-Flow Compressor Stage

Aravinth Sadagopan[1] and Cengiz Camci[2]

*Dept. of Aerospace Engineering, Turbomachinery Aero-heat Transfer Laboratory*

*The Pennsylvania State University, University Park, PA 16802*

**A surge in the small jet engine market due to aero-propulsion purposes generates requirement to develop compact and robust high-performance compressors. We address this necessity through the design of a single-stage high-pressure ratio mixed-flow compressor. Its compactness and reliability demonstrate its ability to replace a multistage axial design in the small aero-engine segment with high-performance envelope. We have perceived that though many design approaches are readily available for centrifugal and/or axial stages, mixed-flow compressor design systems are scarce.**

**In this paper we intend to provide the designer a comprehensive background knowledge of a mixed-flow stage design. A brief historical development of these designs since the 1940s has been provided. It is observed that for a high-pressure ratio demand it necessitates a supersonic rotor exit flow. Hence, tandem stator configurations were investigated in the past to reduce blade loadings for efficient diffusion. However, most of the previous stage designs were inefficient due to inability of the stators to efficiently diffuse this supersonic flow. A tandem design based on Quishi et al. [1] has been implemented to solve this problem.**

**A unique mean-line procedure based on isentropic equations is defined for mixed-flow stage. It is followed by a geometry construction technique based on Bezier curves. Furthermore, a rotor design evaluation study is conducted for 3.5 kg/sec mass flow based on the mean-line code and additional computational analysis. Current computational results [2] have shown single-stage mixed-flow compressors designed using this method to generate reasonably high-pressure ratio up to 6:1 with 75.5% efficiency.**

**Keywords:** Aero-jet engine, compressor, mixed-flow, blade optimization, supersonic flow, tandem diffuser design, first principles, Bezier curves.

[1] *Graduate Research Assistant, Dept. of Aerospace Eng., 47B Hammond Bldg., University Park PA 16802.*

[2] *Professor of Aerospace Eng., ASME Fellow, Dept. of Aerospace Eng., 223 Hammond Bldg., University Park PA 16802.*

## Nomenclature

| | | |
|---|---|---|
| $A$ | = | Area, [$m^2$] |
| $A'$ | = | Area normal to rotational axis, [$m^2$] |
| $b$ | = | Vane-less space depth, [m] |
| C | = | Absolute velocity, [m/s] |
| $C_a$ | = | Axial absolute velocity, [m/s] |
| $C_P$ | = | Specific heat at constant pressure, [$J.(Kg .K)^{-1}$] |
| $CFD$ | = | Computational fluid dynamics |
| $I_m$ | = | Rothalpy, [$J/ Kg^{-1}$], $Cp. T + 0.5(W^2 - U^2)$ |
| $L$ | = | Axial length, [m] |
| $\dot{m}$ | = | Mass flow rate, [Kg/s] |
| $M$ | = | Mach number |
| $M_{rel}$ | = | Relative Mach number |
| $N$ | = | Number of blades |
| $NACA$ | = | National Advisory Committee for Aeronautics, former NASA |
| $P$ | = | Static Pressure, [Pa] |
| $P_o$ | = | Total Pressure, [Pa] |
| $r$ | = | radius, [m] |
| $R$ | = | Gas constant, [Air R=287 J/Kg .K] |
| $RPM$ | = | Revolutions per minute |
| $S$ | = | Blade pitch |
| $t$ | = | pitch wise distance between B1 and B2 |
| $temp$ | = | temporary variable |
| $T$ | = | Static Temperature, [K] |
| $T_o$ | = | Total Temperature, [K] |
| $U$ | = | Tangential blade velocity, [m/s] |
| $UAV$ | = | Uninhabited air vehicle |
| $W$ | = | Relative velocity, [m/s] |
| $X$ | = | Axial location, [m] |
| $\Delta$ | = | Control point |
| $\phi$ | = | Flow coefficient |
| $\gamma$ | = | Specific heat ratio |
| $\rho$ | = | Density, [$kg/m^3$] |
| $\eta_{IS}$ | = | Isentropic efficiency (total-to-total) |
| $\Pi_{TT}$ | = | Pressure ratio (total-to-total) |
| $\Omega$ | = | Angular rotational speed, [rad./s], design value=28,500 RPM |
| $\Phi$ | = | Meridional angle, [degrees] |
| $\beta$ | = | Blade angle, [degrees] |
| $\alpha$ | = | Flow angle, [degrees] |
| $\lambda$ | = | Wedge angle, [degrees] |
| $\tau$ | = | Airfoil thickness |

## Subscripts

| | | |
|---|---|---|
| *t* | = | Tip |
| *h* | = | Hub |
| *m* | = | Mid |
| *B1* | = | Stator blade row 1 |
| *B2* | = | Stator blade row 2 |
| *R* | = | Rotor |
| *VS* | = | Vane-less space |
| *S* | = | Stator |
| *1* | = | Rotor inlet station |
| *2* | = | Rotor exit station |
| *3* | = | Stator inlet station |
| *4* | = | Stator exit station |

# I. Introduction

Small aero-engine market has seen an enormous growth in the past decade with advent of UAVs in a wide variety of applications. Piston engines dominated this segment because of the lack of availability of high-performance and cost-effective small jet engines. With the current technological expertise in gas turbines a highly loaded compact jet engine with high altitude operational capability will bridge this gap. Improvisation of the conventional jet engine designs with reduced mechanical component volume and weight will lead to higher reliability, reduced component manufacturing costs and improved engine life-cycle. Since at the core, engine performance and efficiency cycle depend majorly on the compressor, it necessitates further development of compact high-performance compression systems.

Previously, to address this issue centrifugal compressor designs with high stage pressure ratios have been developed, but their main drawback was an inherent large frontal diameter mainly due to the radial diffuser. This relatively large diameter limits their usage in aircraft propulsion applications. On the contrary, an axial flow compressor requires a longer axial length with multi-stage necessity to pitch in the same overall pressure ratio. A mixed-flow single stage design with smaller frontal area and higher pressure ratio is an effective solution to these problems. It provides the robustness and work level of a centrifugal in a much shorter length than that of a multi-stage axial compressor. Reduced stage-number property of the mixed flow design for the same compression ability leads to significant cost reduction in manufacturing, possible reliability improvement and reduced maintenance time/cost. The mixed-flow compressor could handle foreign object damage and flow distortion in a better way compared to the axial design. The shorter system length and reduced weight when compared to an axial design is highly beneficial. A complete single stage mixed-flow compressor solid model obtained from the current design methodology is shown in ***Figure 1.***

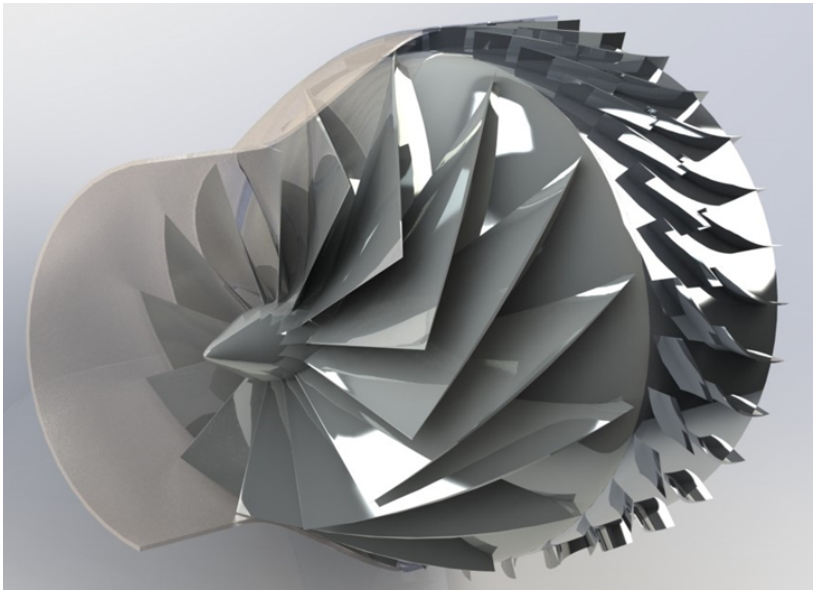

*Figure 1 A 6:1 Mixed-flow compressor stage solid model obtained from the current design methodology*

The first mixed-flow design to be experimentally evaluated, was by *King and Glodeck* (1942) [3]. It was followed by a series of experiments conducted by the NACA during 1950-60s. *Wilcox and Robbins* (1951) [6] incorporated a supersonic diffuser with bleed air to improve stage performance. It suffered significant total pressure losses occurring due to poor flow distribution and mixing. Blade wakes and shock losses equally contributed to the inefficiency of this diffuser.

Pump, turbocharger and UAV applications slowly propelled mixed-flow design developments for the next 3 decades. During the 1980s, *Dodge* (1987) [9] patented design conceived a mixed-flow impeller as an inlet transonic fan. A 3-stage axial flow compressor was found to be replaceable by a single stage 3:1 mixed-flow design by *Musgrave and Plehn* (1987) **[10].** Another design providing an impeller total pressure ratio of $\Pi_{TT}$ =7.5:1 by *Eisenlohr and Benfer* (1994) [11] with a high $\mathbf{r_{2m}/r_{1m}}$ ratio and splitter blade suffered from overall stage loss with tandem type diffuser. *Elmendorf et al.* (1995) [12] conducted an extensive study with the prospect of mixed-flow design's applicability in small jet engines. Their 5:1 shock-in-rotor configuration developed with shock stabilizing technique was combined with a supersonic tandem type diffuser. Even this development resulted in a diffuser with reduced overall stage performance. Thus, the impeller exit Mach number proves to be very crucial quantity to define an efficient diffuser design.

The potential of a single stage mixed-flow design as an aircraft compressor is realizable, but all these designs suffered from shock losses in the diffuser paying a heavy penalty for the stage efficiency. Primarily to overcome this limitation, *Youssef* (2002) **[13]** resorted to a subsonic mixed-flow compressor stage. The patented design has a 2-stage mixed-flow compressor claiming to achieve an overall stage $\Pi_{TT}$ of 10-13.

More recently, an impeller tip clearance study conducted by *S. Ramamurthy et al.* (2009) **[17]** describes an early surging with higher tip clearance due to an unsteady interaction of the main flow with the leakage flow. The study states that constant tip clearance gives better performance over variable tip clearance. It also states that the typical jet wake flow in radial machines is absent in the mixed-flow configuration in addition to the absence of recirculation at the inlet. The stage design yielded $\Pi_{TT}$ of 4.55 with $\eta_{IS}$ of 80% for $\dot{m}$ of 3.3-3.36 kg/s. A robust design optimization study by *Cevik et al.* (2009) **[19]** determines that the mixed-flow impeller performs better for a small jet engine compared to a small radial compressor. The study minimizes the cost function based on specific thrust and TSFC.

A critical study on blade loading distribution of the mixed-flow impeller was done by *Xuanyu et al.* (2014) **[16].** This study concludes that an increased blade loading at the hub's posterior area is desired for a better performance due to control on the hub flow separation and more adaptable to the changing flow passage. Similarly, an increased frontal tip section loading would make the impeller achieve a higher total pressure ratio in surging conditions. With a mass flow of 18 kg/s, this stage design achieves a $\Pi_{TT}$ of 2.72.

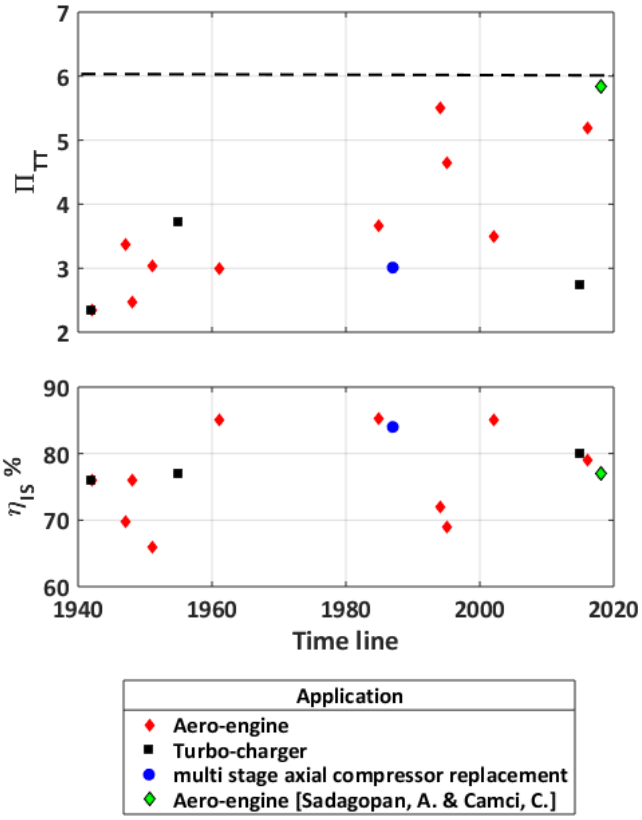


*Figure 2 Past designs points of mixed-flow compressors (green diamond is current design)*

*Giri et al.* (2016) [15] designed a mixed-flow impeller, diffuser followed by an axial stator. Impeller inlet and exit end wall contour design was optimized to minimize losses. The splitter blade length was extended to obtain a higher $\Pi_{TT}$. Providing pre-swirl at the impeller inlet improved the efficiency by reducing the inlet Mach number and attenuated losses which occured due to high inlet velocities. The design achieved a $\Pi_{TT}$ of 5.2 with $\eta_{IS}$=79.1% for a $\dot{m}$ of 1.74 kg/s. Most of the past mixed-flow design performances including the current design are presented in *Figure 2*. *Figure 3* shows pressure ratio versus stage efficiency information for all designs in *Figure 2*. Based on *Figure 3*, it is observed that obtaining a high-pressure ratio and efficiency simultaneously for a single stage is quite challenging. There are only two mixed-flow designs over the pressure ratio of $\Pi_{TT}$ =5 out of 14 past designs. The present design has the highest pressure ratio near $\Pi_{TT}$ =6 at an elevated engine mass flow rate of 3.5 kg/s. There are only four past mixed-flow designs with an efficiency $\eta_{IS}$ value over 80%. However, all of these four designs exhibited a pressure ratio of less than 3.7. The current design generates a pressure ratio $\Pi_{TT}$ in the vicinity of 6 at an engine mass flow rate of 3.5 kg/s with a total to total efficiency of $\eta_{IS}$ =75.5 %.

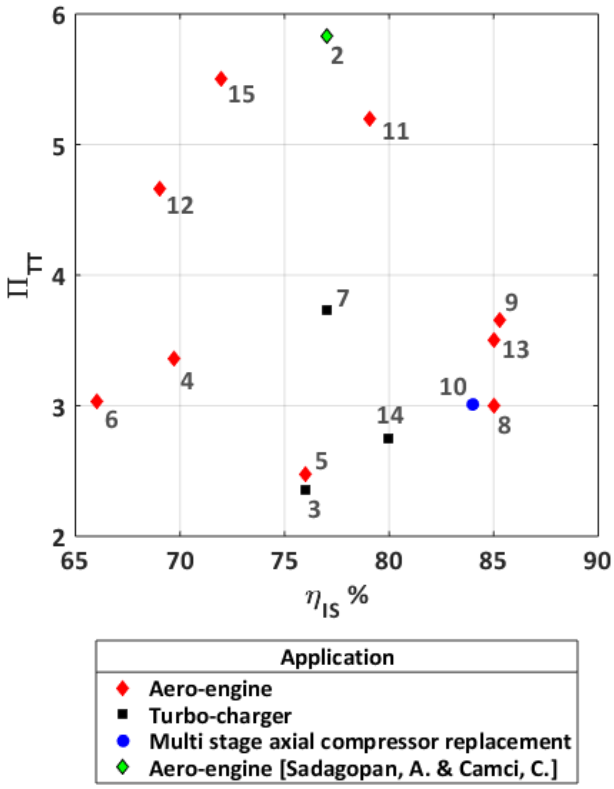


*Figure 3 Pressure ratio vs efficiency of mixed-flow compressors at design point, numbers [2-15] denote the work cited in references.*

The authors aim to achieve a relatively high $\Pi_{TT}$ near 6 in a single-stage for a $\dot{m}$ of 3.5 kg/s within 400mm maximum outer diameter. Since, most of the earlier designs suffered from poor stator performance, the main challenge is the recovery of stagnation pressure with a high isentropic efficiency in the presence of supersonic inlet and large turning angle in the stator. To reduce the blade loading in a single-stator row, many investigators utilized tandem designs for both subsonic and supersonic cases in the past. However, past performances of the supersonic tandem stators were not satisfactory. Recently, *Quishi et al.* (2010) [1] proposed and investigated a highly loaded supersonic tandem stator with 2 cascade rows based on aspirated-fan concept. The first row of the cascade having a supersonic airfoil reduced the flow into a subsonic one and the second row provides the large flow turning immersed in a subsonic domain. Losses were minimized when leading edge of the second row lied close to pressure side of first row at 20% pitch-to-pitch distance with no axial spacing or overlapping in the axial direction. Incorporation of this design feature in tandem type stator design for a mixed-flow compressor could provide relatively high stage pressure ratio and efficiency in a single stage.

Most of the available commercial design codes contain undisclosed procedures which are heavily dependent on the code developer's intuition and experience. They do not provide complete understanding and clarity to the user. Many mean-line design illustrative procedures are available for centrifugal and axial compressor stages, but very few attempts were made on mixed-flow stage designs. The main objective of this paper is to provide strategic guidance to design a high-pressure ratio and high-performance mixed-flow compressor. A simple mean-line procedure is defined to relate mixed-flow compressor geometric and aero-thermal parameters to the specific design requirements. A rotor mean-line design procedure is followed by a unique tandem stator design. It is succeeded by the corresponding design geometry generation procedure primarily based on Bezier curves. Finally, a detailed design evaluation study is conducted for the mixed-flow rotor and the tandem stator. The performance results of the present mixed flow design including viscous flow features, compressibility issues, shock waves and resulting aerodynamic losses are dealt with in a subsequent paper by *Sadagopan and Camci* [2].

## II.Mean-line Rotor Design Procedure

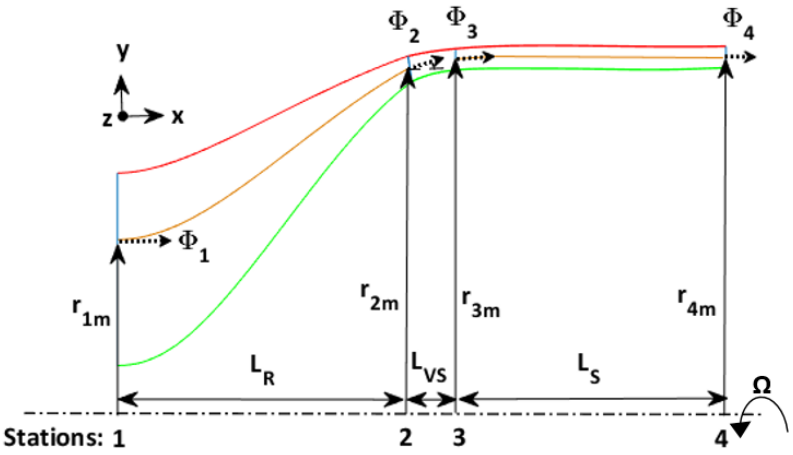


***Figure 4 Meridional view of the stage showing ϕ, L and r definitions.***

The meridional view of a mixed-flow stage is described in *Figure 4*. Inlet geometric parameters at station '1' are defined using the design point specifications. Operational altitude and compressor inlet Mach number ($M_1$) provide free stream density ($\rho_1$) and inlet velocity ($C_1$). Design mass flow rate ($\dot{m}$) fixes the inlet area ($A_1$) using continuity equation. It is deducible that a higher $A_1$ is needed with altitude to accommodate same $\dot{m}$ through the engine. Inlet meridional angle ($\Phi_1$) could be varied depending upon the compressor stage application.

*Eqn. (1)* relates hub radius $\mathbf{r_{1h}}$ and tip radius $\mathbf{r_{1t}}$ for a given $\dot{m}$. Having a lower $\mathbf{r_{1h}}$ is beneficial because it increases $\mathbf{r_{2m}}$/ $\mathbf{r_{1m}}$ ratio, hence the rotor $\Pi_{TT}$. However, $\mathbf{r_{1h}}$ is limited based on structural/design constraints of the shaft for the chosen RPM and $\mathbf{r_{1h}}$/ $\mathbf{r_{1t}}$ ratio for the blade structure. The mean radius $\mathbf{r_{1m}}$ splits the inlet area $A_1$ based on $\dot{m}$.

$$r_{1t} = \sqrt{\left(\frac{\pi\,\dot{m}}{4\,C_1\,\rho_1}\right) + r_{1h}^2} \tag{1}$$

RPM is evaluated by limiting the inlet tip relative Mach number ($M_{1t\,rel.}$). Based on [20], $M_{1t\,rel.}$ around 1.4 ~1.5 is typically chosen to minimize losses due to passage shock. *Eqn. (2-4)* developed from the inlet velocity triangle are used to obtain shaft rotational rate Ω.

$$\beta_{1t} = cos^{-1}\left(\frac{Ca_{1t}}{W_{1t}}\right) \tag{2}$$

$$U_{1t} = Ca_{1t}\,tan(\beta_{1t}) \tag{3}$$

$$\Omega = \frac{U_{1t}.\,60}{2.\,r_{1t}.\,\pi} \tag{4}$$

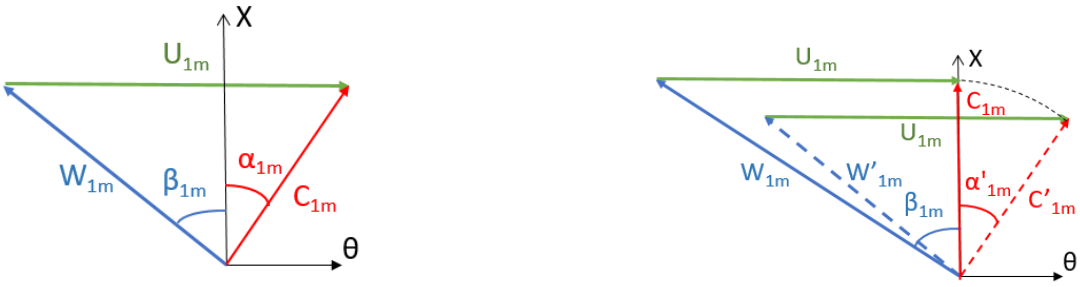


***Figure 5 Rotor inlet velocity triangle at mean radius $r_{1m}$ showing the benefits of swirl flow.***

***$C'_{1m} = C_{1m}$; $U_{1m}$ is the same; $W'_{1m} < W_{1m}$***

Flow swirling at rotor inlet reduces $M_{1rel}$ and benefits the rotor efficiency by curtailing passage shock losses. This effect is seen in ***Figure 5***, the inlet velocity triangle at $\mathbf{r_{1m}}$. The challenge with this configuration is designing a

transonic airfoil with high total pressure recovery and flow turning capability. At this point, all the inlet rotor blade parameters, including inlet blade angles ($\beta_1$) are characterized at hub, mean and tip radius locations.

Rotor exit parameters '2' are obtained along the mean-line. Total pressure and temperature at rotor exit for design point pressure ratio $\Pi_{TT}$ and approximated $\eta_{IS}$ are found using the definition of isentropic total-to-total efficiency, *eqn. (5)*.

$$T_{o2} = T_{o0} + (\Pi_{TT}^{(\gamma-1)/\gamma} - 1).\ (T_{o0}/\eta_{IS}) \quad (5)$$

Then the exit Mach number $M_2$ is approximated in the range of 1 → 1.4 to get the exit static parameters with *eqn. (6-8)*.

$$T_2 = T_{o2} / (1 + 0.2\, M_2^2) \quad (6)$$

$$P_2 = P_{o2} / (T_{o2}/T_2)^{(\gamma/(\gamma-1))} \quad (7)$$

$$\rho_2 = P_{o2} / (R.\ T_{o2}.\ (1 + 0.2\, M_2^2)^{(1/(\gamma-1))} \quad (8)$$

$$I_{m1} = Cp.\ T_1 + 0.5.\ (W_{1m}^2 - U_{1m}^2) \quad (9)$$

$$I_{m2} = I_{m1} \quad (10)$$

$$U_{2m} = \Omega . r_{2m} \quad (11)$$

$$W_{2m} = \sqrt{I_{2m} - Cp.T_2 + U_{2m}^2} \quad (12)$$

Rothalpy conservation principle between rotor inlet and exit along the mean-line *eqn. (9-10)* is used to connect rotor inlet and exit stations. $C_{2m}$ is obtained using the approximated $M_2$ and $a_2$. $W_{2m}$ and $U_{2m}$ are a function of $r_{2m}$ *eqn. (11-12)*. $M_{2rel}$ is approximated to determine an $\mathbf{r_{2m}}$ value. Since it is an iterative procedure, detailed parametric analysis is mentioned in ***Section VI***. A chosen $\mathbf{r_{2m}}$ value is used to obtain $\alpha_{2m}$ and $\beta_{2m}$ and the exit velocity triangle at mean radial location is derived as shown in ***Figure 6.***

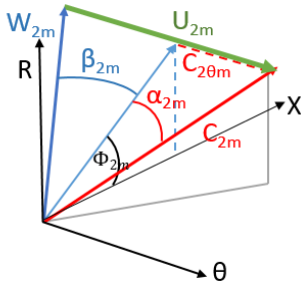


*Figure 6 Rotor exit velocity triangle at mean radius, r2m.*

A positive $\beta_{2m}$ is desired since back sweep provides more rotor stability [21]. The meridional exit angle ($\Phi_2$) and rotor axial length ($L_R$) are chosen as described in ***Section VI.*** $\mathbf{r_{2t}}$ and $\mathbf{r_{2h}}$ are evaluated again using continuity equation and meridional exit angle ($\Phi_2$), *eqn. (13-17).* Similar procedure is followed to characterize exit hub and tip velocity triangles. Kantrowitz limit does not play a role in this design process as passage area is not evaluated.

$$C_{a2m} = C_{2m}.cos\ (\alpha_{2m}) \tag{13}$$

$$A'_2 = \dot{m} / (\rho_2.\ C_{a2m}) \tag{14}$$

$$r_{2h} = \sqrt{r_{2m}^2 - \frac{A'_2.\ cos\ (\Phi_2)}{2.\pi}} \tag{15}$$

$$r_{2t} = \sqrt{2.r_{2m}^2 - r_{2h}^2} \tag{16}$$

$$A_2 = \frac{\pi}{cos(\Phi_2)}.(r_{2t}^2 - r_{2h}^2) \tag{17}$$

## III.Mean-line Stator Design Procedure

Exit Mach number $M_2$ from rotor exit is supersonic but it has subsonic radial, tangential and axial components for the current design, *eqn. (18-20).*

$$M_{2\theta} = M_2 . Sin\ (\alpha_{2m}) \quad (18)$$

$$M_{2r} = M_2 . Sin\ (\Phi_2) . Cos\ (\alpha_{2m}) \quad (19)$$

$$M_{2x} = M_2 . Cos\ (\Phi_2) . Cos\ (\alpha_{2m}) \quad (20)$$

Stagnation enthalpy is assumed to be conserved in the vane-less space (VS) along the mean-line, hence $T_{o3} = T_{o2}$. Then according to the initial isentropic flow approximation; $P_{o3} = P_{o2}$. The hub and casing radius in the vane-less space is designed to reduce the cross-sectional area in the axial direction to diffuse the supersonic flow. Their curvature is designed to turn the radial velocity component to the axial direction. The axial length ($L_{VS}$) in this region determines the rotor stator interaction. A length exceeding 15 mm generates a normal shock in the vane-less spacing. Since this region is attempting to diffuse a supersonic flow any increment in length will correspond to shock instability. A very low $L_{VS}$ value is acoustically undesirable.

The radial vane-less diffusion follows conservation of mass and momentum equations, showing that the flow angle depends on the density and passage depth based on Japikse and Baines **[22]**. Since the current design incorporates varying VS depth (b) and ρ (compressibility effect), $\alpha_{3m}$ will vary from $\alpha_{2m}$ as seen in *eqn. (21-22).*

$$r_m . C_\theta = const. \quad (21)$$

$$\tan(\alpha) = \frac{C_\theta}{C_m} = (const. \rho b)/\dot{m} \quad (22)$$

Area ratio ($A_3/A_2$) is obtained using the isentropic area *eqn. (23)* by specifying a $M_3$ value. The values $\Phi_3$ and $\mathbf{r_{3m}}$ are specified based on the rotor exit meridional angle $\Phi_2$ and mean radius $\mathbf{r_{2m}}$. $\mathbf{r_{3h}}$ and $\mathbf{r_{3t}}$ are then extracted using continuity equation, *eqn. (24-25).* In this case the value of $\mathbf{r_{3m}}$ is higher than $\mathbf{r_{2m}}$. Choice of $\Phi_3$ depends on how the vane-less space is intended to perform. A positive meridional angle $\Phi_3$ will lead to enhanced diffusion due to increasing mean radius with the same $L_{VS}$ but $\Phi_3$ is chosen closer to $0^o$ due to the outer diameter constraints. This leads to a two-dimensional inlet for the vaned stator with $M_{3\theta}$ and $M_{3x}$ components obtained from *eqn. (26-27).*

$$\frac{A_3}{A_2} = \frac{M_2}{M_3}.\left[\frac{1+\frac{(\gamma-1)}{(\gamma+1)}.(M_3^2)}{1+\frac{(\gamma-1)}{(\gamma+1)}.(M_2^2)}\right]^{\frac{(\gamma+1)}{2(\gamma-1)}} \quad , where, \quad \frac{A_3}{A_2} < 1 \tag{23}$$

$$r_{3h} = \sqrt{r_{3m}^2 - \frac{A_3.\ cos\,(\Phi_3)}{2.\pi}} \tag{24}$$

$$r_{3t} = \sqrt{r_{3m}^2 + \frac{A_3.\ cos\,(\Phi_3)}{2.\pi}} \tag{25}$$

$$M_{3x} = M_3.cos\,(\alpha_{3m}) \tag{26}$$

$$M_{3\theta} = M_3.\ sin\,(\alpha_{3m}) \tag{27}$$

The objective for a stator in this design approach is to diffuse the incoming supersonic flow, to turn it to axial direction and recover maximum stagnation pressure within the external diameter and axial length constraints. After analyzing a number of possible supersonic diffuser configurations, we decided to proceed with a tandem stator configuration based on aspirated-fan designs [23]. The tandem diffuser uses two blade rows with the first row diffusing supersonic flow and the second row turning and diffusing subsonic flow. Stator inlet parameters are assessed from the VS exit mean-line values. A detailed description of this stator design is mentioned in *Sadagopan and Camci* [2]. The crucial quantities to be determined to design this component are the inlet-exit area ratio ($A_4/A_3$) and the axial length ($L_S$). Stator vanes are required to turn the tangential velocity component to an axial and diffuse it. $M_4$ is chosen in the range of 0.3-0.5 and exit area $A_4$ is evaluated based on *eqn. (23)* using station 3 values. $\mathbf{r_{4m}}$ is chosen to be equal to $r_{3m}$. $\mathbf{r_{4m}}$ could be higher than $\mathbf{r_{3m}}$ which in turn will aid in radial diffusion if stage external diameter is not a constraint. It is a design choice based on the application. However, we chose $\alpha_{4m}$ as $0^o$. $\mathbf{r_{4h}}$ and $\mathbf{r_{4t}}$ are obtained from $\mathbf{r_{4m}}$ and $A_4$ values using *eqn. (24-25).* $L_S$ is chosen as 150mm for our case based on the tandem stator aspect ratio definition in [1]**.** Stagnation enthalpy is assumed to be conserved across stations 3 and 4. Using this the static terms at station 4 are determined using the isentropic equations.

## IV. Rotor geometry definition

The rotor camber line at hub, mean and tip sections is constructed using a Bezier curve. Blade parameters characterized in ***section I*** are used as the input to define this curve. A 3rd order curve is chosen due to the availability of 4 definitive points for each section. The usage of Bezier polynomial is sought for simplification. The difference between B-spline and Bezier for this degree would be minimal. X, Y and Z definition for each point is geometrically derived using the mean-line parameters. H, M and T, *eqn. (41-43)* each represent the individual 3x4 matrix of the

XYZ points for corresponding Bezier Curve. 3rd order Bernstein Matrix is then multiplied with each of H, M and T matrix to obtain the three curves generated in the range of 0 to 1 to get the camber line shape shown in *Figure 7*.

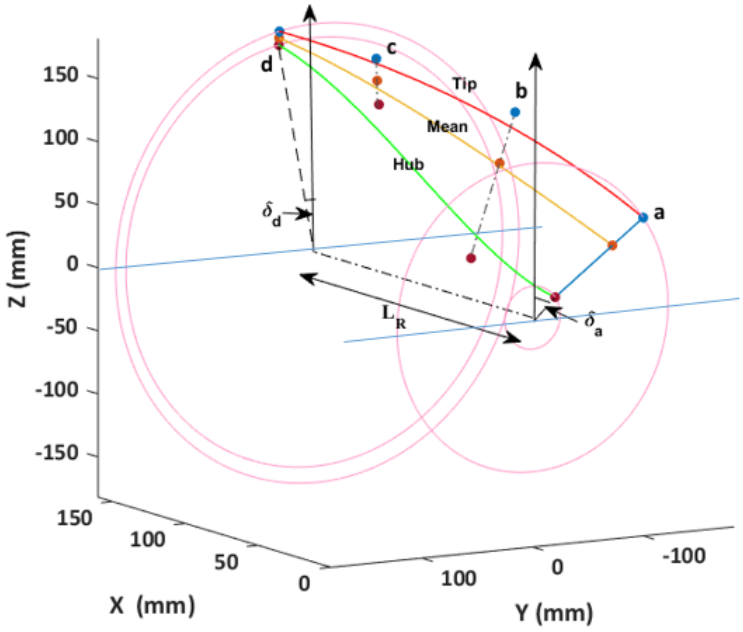


***Figure 7 Rotor mean camber lines defining hub, mean and tip section using Bezier curve. Corresponding control points a, b, c and d.***

Point 'a' at H, M and T is defined by inlet **r** value and $\delta_a$ using *eqn. 28* where $\Delta_1$ is hub X location of point 'b'. $\Delta_1$ location is kept in 20-30% of the total rotor axial length '$L_R$'. T and M 'X' location is given by *eqn. (29-30)*. $\Delta_3$ is a control factor used to adjust point 'b' location, usually it is in the range of 1→3. Row 2 of H, M and T matrices show the X, Y and Z definitions for point 'b'. *Figure 8* shows the geometric definition for points 'a' and 'b'.

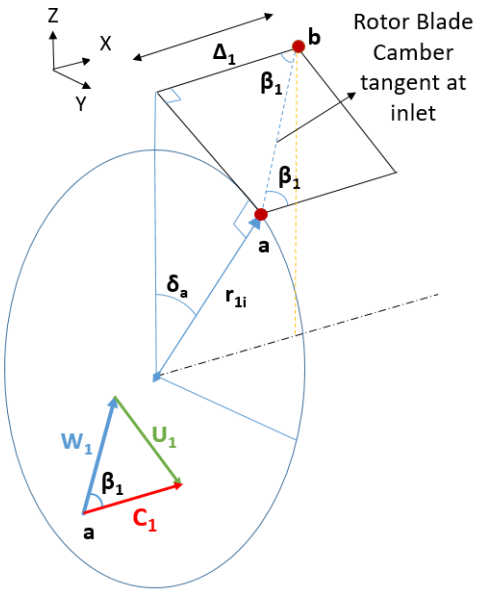


*Figure 8 Control points 'a' and 'b' with the inlet velocity triangle at 'a'.*

$$\delta_a = tan^{-1}\frac{\Delta_1.tan(\beta_{1h})}{r_{1h}} \quad (28)$$

$$X_{bm} = r_{1m}.\frac{tan\,\delta_a}{tan\,\beta_{1m}} \quad (29)$$

$$X_{bt} = r_{1t}.\frac{tan\,\delta_a}{tan\,\beta_{1t}} \quad (30)$$

$$temp_{0i} = \sqrt{(r_{1i}.tan\,\delta_a)^2 - (r_{1i}.tan\,\delta_a)^2} + r_{1i}.cos\,\delta_a + \Delta_1.cos\,\beta_{1h}.\ tan\,\Phi_{1i},\quad where\ i=h,\ m\ and\ t. \quad (31)$$

$$\delta_d = tan^{-1}\frac{(L_R-\Delta_2).tan\,(\beta_{2h})}{r_{2h}} \quad (32)$$

$$X_{ch} = L_R - \Delta_2 \quad (33)$$

$$X_{cm} = r_{2m}.\frac{tan\,\delta_d}{tan\,\beta_{2m}} \quad (34)$$

$$X_{ct} = r_{2t}.\frac{tan\,\delta_d}{tan\,\beta_{2t}} \quad (35)$$

$$temp_{1i} = \sqrt{(r_{2i}.tan\,\delta_d)^2 - (r_{2i}.sin\,\delta_d)^2} + r_{2i}.cos\,\delta_d \quad (36)$$

$$temp_{2i} = tan\,\Phi_{2i}.\sqrt{(X_{ci})^2 + (r_{2i}.sin\,\delta_d)^2 + (r_{2i}.cos\,\delta_d - temp_{1i})^2} \quad (37)$$

$$temp_{3i} = \frac{r_{2i}.cos\,\delta_d - temp_{1i}}{r_{2i}.sin\,\delta_d} \quad (38)$$

$$Y_{ci} = \sqrt{\frac{(temp_{2i}.temp_{3i})^2}{1+temp_{3i}^2}} \tag{39}$$

$$Z_{ci} = temp_{1i} + \frac{Y_{ci}}{temp_{3i}} \tag{40}$$

$$H = \begin{bmatrix} 0 & -r_{1h}.\sin\delta_a & r_{1h}.\cos\delta_a \\ \frac{\Delta_1}{\Delta_3} & -r_{1h}.\frac{\sin\delta_a}{\Delta_3} & \frac{(temp_{0h}+r_{1h}.\sin\delta_a)}{\Delta_3} \\ X_{ch} & Y_{ch} & Z_{ch} \\ L_R & r_{2h}.\sin\delta_d & r_{2h}.\cos\delta_d \end{bmatrix} \tag{41}$$

$$M = \begin{bmatrix} 0 & -r_{1m}.\sin\delta_a & r_{1m}.\cos\delta_a \\ \frac{X_{bm}}{\Delta_3} & -r_{1m}.\frac{\sin\delta_a}{\Delta_3} & \frac{temp_{0m}+r_{1m}.\sin\delta_a)}{\Delta_3} \\ L_R - X_{cm} & Y_{cm} & Z_{cm} \\ L_R -(r_{2m}-r_{2h}).tan(\Phi_2) & r_{2m}.\sin\delta_d & r_{2m}.\cos\delta_d \end{bmatrix} \tag{42}$$

$$T = \begin{bmatrix} 0 & -r_{1t}.\sin\delta_a & r_{1t}.\cos\delta_a \\ \frac{X_{bt}}{\Delta_3} & -r_{1t}.\frac{\sin\delta_a}{\Delta_3} & (temp_{0t}+r_{1t}.\frac{\sin\delta_a)}{\Delta_3} \\ L_R - X_{ct} & Y_{ct} & Z_{ct} \\ L_R -(r_{2t}-r_{2h}).tan(\Phi_2) & r_{2t}.\sin\delta_d & r_{2t}.\cos\delta_d \end{bmatrix} \tag{43}$$

In a similar way of definition point 'd' uses *eqn. 32* defined by $\delta_d$ and $r_2$ values. $\Delta_2$ is the hub X location of point 'c'. It is kept around 80-90% of $L_R$. X location for 'c' tip and mean are obtained from *eqn. (33-35)*. As the exit is oriented at a meridional angle the definitions for Y and Z location for 'c' is given in *eqn. (36-40)*. The two intermediate point locations are controlled using $\Delta_1$ and $\Delta_2$ to adjust the blade curvature. A low camber variation in the tip section helps to avoid flow separation. $\Phi_{2i}$ are the meridional angles at hub, mean and tip specified according to the rotor exit and vane-less spacing interaction. Using these point definitions 3 camber lines for H, M and T are generated. The chosen airfoil thickness is distributed along the Bezier curve camber perpendicular to local camber direction to get the rotor hub, mean and tip airfoil sections. The slope variation of the camber curve is obtained from the Bezier X, Y and Z coordinates. The airfoil thickness and axial locations are non-dimensionalized and then converted to the rotor dimensions based on $L_R$. NACA 65-206 series airfoil is chosen for this mixed-flow rotor. Due to extreme stretching, the original behavior of the airfoil is difficult to preserve. In this case, the same airfoil with

thickness percentage varying from 75(hub), 50(mean) and 35(tip) % are used to obtain the 3-dimensional mixed-flow rotor. Finally ***Figure 9*** describes a 3D mixed-flow rotor generated with the given geometric conditions.

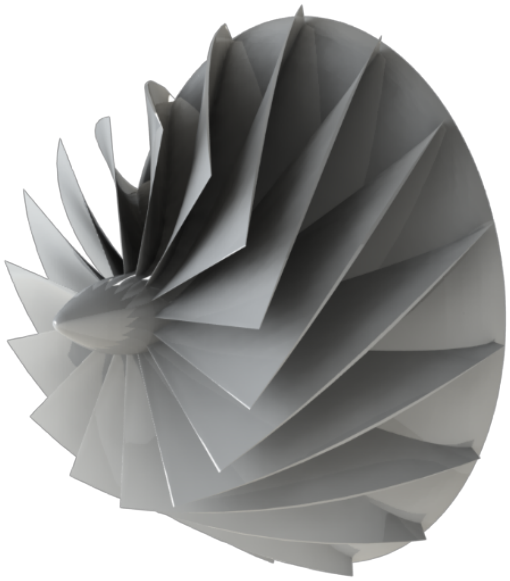

***Figure 9 Final 3D solid model of a mixed-flow rotor after the airfoil addition to camber sheet.***

## V. Stator geometry definition

The preliminary level of design involves tandem stator row definition in a two-dimensional plane. $\alpha_{3m}$ is considered as the inlet flow angle. Exit flow is oriented in the axial direction. A 3rd order Bezier Curve using the inlet ($\alpha_1$) and exit ($\alpha_2$) stator angles defines the camber line. The percentage axial length of each blade row is chosen to determine the axial length of blade row 1 ($L_{B1}$). $X_{LB1}$ is the axial location of the leading edge of $B_1$. Three location control points $\Delta_1$, $\Delta_2$ and $\Delta_3$ are used to manually define the mean camber. Matrix $P_{B1}$, *eqn. (44)* contains the Bezier curve defining points shown in ***Figure 10***. It is important to remember that the first blade row's main purpose is to diffuse the supersonic flow using oblique and passage shocks effectively. Thus, the blade turning angle ($\alpha_1 - \alpha_2$) is limited in the range of 7-10° to avoid excessive shock boundary layer separation losses.

$$P_{B1} = \begin{bmatrix} X_{LB1} & 0 & 0 \\ X_{LB1} + \Delta_1 & -\tan(\alpha_I).\Delta_1 & 0 \\ X_{LB1} + L_{B1} - \Delta_2 & -\Delta_3 + \Delta_2.\tan(\alpha_2) & 0 \\ X_{LB1} + L_{B1} & -\Delta_3 & 0 \end{bmatrix} \quad (44)$$

**$C_{B1}$ = B. $P_{B1}$** where B is Bernstein polynomial of order 3.

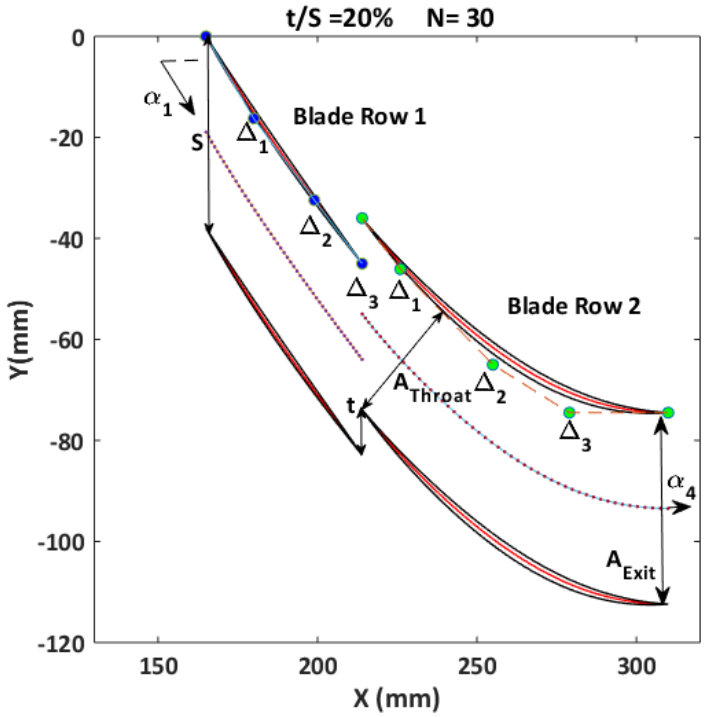


*Figure 10 2D stator construction using the control points and inlet, exit flow angles.*

A 3rd order polynomial function, *eqn. (45)* defines the airfoil thickness. The inlet ($\lambda_i$) and exit ($\lambda_e$) wedge angles need to be specified based on supersonic inlet Mach number ($M_3$) and oblique shock positioning. $\Delta_1$ and $\Delta_2$ are the two control points which adjust the thickness distribution based on the design. P is the airfoil thickness distribution function shown in ***Figure 11*** which is wrapped on the camber line to obtain the stator blade airfoils. Coefficients are defined by *eqn. (46-48).* Thickness (P) is distributed perpendicular to camber curve's slope. Different thickness distributions '$\tau_1$' and '$\tau_2$' are used on the pressure and suction side depending on the shock structure location.

$$P = U_1 r^3 + U_2 r^2 + U_3 r + U_4, \text{ where } r = 0{:}100 \qquad (45)$$

(46)

| | | | |
|---|---|---|---|
| $X_1 = Y_1 = 0$ | $X_2 = C_1;\ Y_2 = X_2 . \tan(\lambda_i)$ | $X_3 = C_2;\ Y_2 = (X_4 - X_3) . \tan(\lambda_e)$ | $X_4 = 100;\ Y_4 = 0$ |

$$F = \begin{bmatrix} 0 & 0 & 0 & 1 \\ X_2^3 & X_2^2 & X_2 & 1 \\ X_3^3 & X_3^2 & X_3 & 1 \\ X_4^3 & X_4^2 & X_4 & 1 \end{bmatrix} \qquad (47)$$

$$U_i = F^{-1} . [Y_A{}^T] \quad \text{where} \quad Y_A = [Y_1\ Y_2\ Y_3\ Y_4] \qquad (48)$$

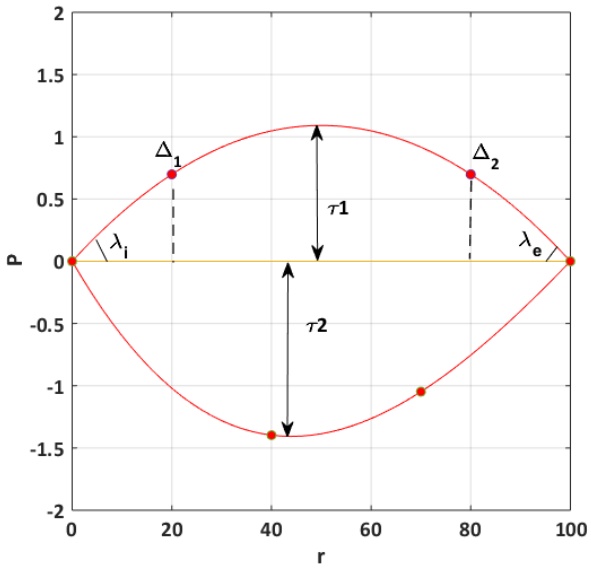


*Figure 11 Polynomial function 'P' distributing airfoil thickness.*

Based on CFD analysis that is described in a subsequent paper by *Sadagopan and Camci* [2], it is observed that flow is well guided by the first blade row, hence we choose the leading edge of the second blade row to be a wedge-shaped profile. For the subsonic profile, the trailing edge radius is indicted in the polynomial thickness distribution for blade 2. Then a similar procedure as performed for row 1 is repeated for blade row 2 camber line construction. Thickness distribution for the suction and pressure side is separately determined by a 3rd order polynomial. 'S' is the blade pitch and 'N' is the blade count for each row. The leading edge is shifted by distance 't' in the pitch wise direction away from the pressure side of blade 1. 't/S' ratio is maintained close to 20% based on [1]. Since this blade row handles a subsonic profile, it is associated with a large flow turning angle ($\alpha_3 - \alpha_4$) ~ (37-40°). Throat and exit area signify the amount of diffusion carried out by this blade row. $\alpha_3$ is equal to $\alpha_2$. $\alpha_4$ is 0° as the exit flow is oriented with the axial direction. The mean camber line is defined by a 4th order polynomial with 3 control points $\Delta_1$, $\Delta_2$ and $\Delta_3$. $\Delta_1$ is defined based on the tangent $\alpha_3$ and t. $\Delta_3$ has the same y value based on the trailing edge location to maintain $\alpha_4$ as 0°. Axial location of the points $\Delta_1$, $\Delta_3$ and $\Delta_2$ are fixed based on the desired camber line curvature.

The stator hub curvature is defined in the meridional plane using a 4th order Bezier Curve starting from the rotor exit. Therefore, $\Phi_{3h} = \Phi_{2h}$, the rotor hub exit meridional angle. $\Phi_{4h} = 0^0$. The casing inlet and outlet meridional angles ($\Phi_{3t}$ and $\Phi_{4t}$) are defined in the same way. 5 control points are used to define each of the hub and casing Bezier curves. $\Delta_{1h}$ is obtained from the rotor hub exit meridional point $r_{2h}$. Axial location of $\Delta_{5h}$ is fixed based on the 2D cascade

design blade 2 exit location given by $L_S$. Y location of $\Delta_{5h}$ is based on $r_{4h}$ value. The Y location for $\Delta_{2h}$ is obtained from $r_{3h}$. It's X location is equal to $L_{VS}$. Y value of $\Delta_{4h}$ is equal to $\Delta_{5h}$. $\Delta_{2h}$ and $\Delta_{4h}$ are defined based on $\Phi_{3h}$ and $\Phi_{4h}$ angles. $\Delta_{3h}$ point is iteratively varied to maintain a smooth profile. The purpose of the X and Y values of $\Delta_{2h}$, $\Delta_{3h}$ and $\Delta_{4h}$ is to obtain the desired camber line curvature. It is an iterative procedure. A similar procedure is followed to obtain $\Delta_{1t\text{-}5t}$, points to define the casing profile.

Finally, ***Figure 12*** defines the three-dimensional stator with the 2D stator design being superimposed on the hub and casing profiles. The Y locations of both the blades in the 2D cascade is converted to radial (r) and angular θ values in the pitch wise direction with the same X (axial location) values.

***Figure 12 Final 3D solid model of a supersonic tandem stator.***

## VI. Rotor Design Evaluation Study

One dimensional mean-line design approach from ***section II*** is used for this parametric study. The design variables are varied to provide a better visualization and clarity to the designer. Primary goal is to get a very high-pressure ratio value greater than 6.0 within an exit external radius ($r_{2t}$) of 180mm. Based on the literature survey and additional computational effort the authors argue that majority of the rotor losses are accounted to casing shock boundary layer interaction and blade leading edge tip region shocks. Secondary flow feature vortices and blade

viscous losses are other two loss generating components in this mixed-flow rotor. To account for all the losses the rotor isentropic efficiency is initially chosen to be 85% for a relative inlet tip Mach number of 1.4. Parameters which are analyzed throughout this exercise are given in *Table 1*. This is only an initial evaluation effort based on an assumed rotor isentropic efficiency of 85%.

**Table 1 Rotor mean-line parametric study variables**

| | |
|---|---|
| $\eta_{IS}$ | 70-100% |
| $M_2$ | 0.5-1.5 |
| $M_{2rel}$ | 0.7-1.2 |
| $r_{2m}$ | 120-220 mm |
| $\dot{m}$ | 3.5 Kg/s |
| $\Omega$ | 28500 RPM |
| $M_1$ | 0.7 |

Rotor inlet Mach no. $M_1$ is 0.7 and inlet relative Mach no. increases from hub to tip with a value of $M_{1trel}$ as 1.4 at the tip section. Based on *Figure 13(a)* if the rotor exit mean radius ($r_{2m}$) and the exit Mach number increase ($M_2$), the rotor pressure ratio ($\Pi_{TT}$) increases. A higher $M_2$ for the same exit radius, efficiency and passage diffusion corresponds to higher pressure ratio. Since the stator inlet Mach number ($M_3$) is limited to be in the range of 1.1~1.3 for a good stator efficiency $M_2$ is chosen to be 1.3. $r_{2m}$ is chosen as 175mm due to the stage external radius constraint of 200mm to provide additional radial gap for the stator section. Lower $M_{2rel}$ denotes more diffusion in the rotor passage. Higher the diffusion in the passage denotes higher amount of work done by the rotor on the fluid which is shown by the high rotor pressure ratio. From *Figure 13(b)* for the same $M_2$ and efficiency value for pressure ratio of 6, $r_{2m}$ and $M_{2rel}$ need to decrease. However, it's not feasible to reduce $M_{2rel}$ due to shock losses and corresponding boundary layer growth due to that adverse pressure gradient. For the same pressure ratio 6 and blade tangential velocity, a lower $M_{2rel}$ corresponds to a lower $M_2$ as seen in *Figure 13(c)*. A higher exit Mach number $M_2$ leads to increase in $M_{2rel}$ and hence increasing efficiency as seen in *Figure 13(d)*. Obtaining a lower $M_{2rel}$ at the same $M_2$ decreases the rotor efficiency as seen in *Figure 13 (d)* and it is very difficult to design a passage which can effectively generate high pressure ratio and perform this diffusion as perceived in *Figure 13(b)*. In conclusion, a higher rotor exit Mach number, higher exit mean radius and low rotor exit relative Mach number is desired to obtain a high-pressure ratio. To increase the isentropic efficiency for the same pressure ratio $M_2$ and $M_{2rel}$ should increase. Rotor back pressure increase corresponds to rotor pressure ratio increment.

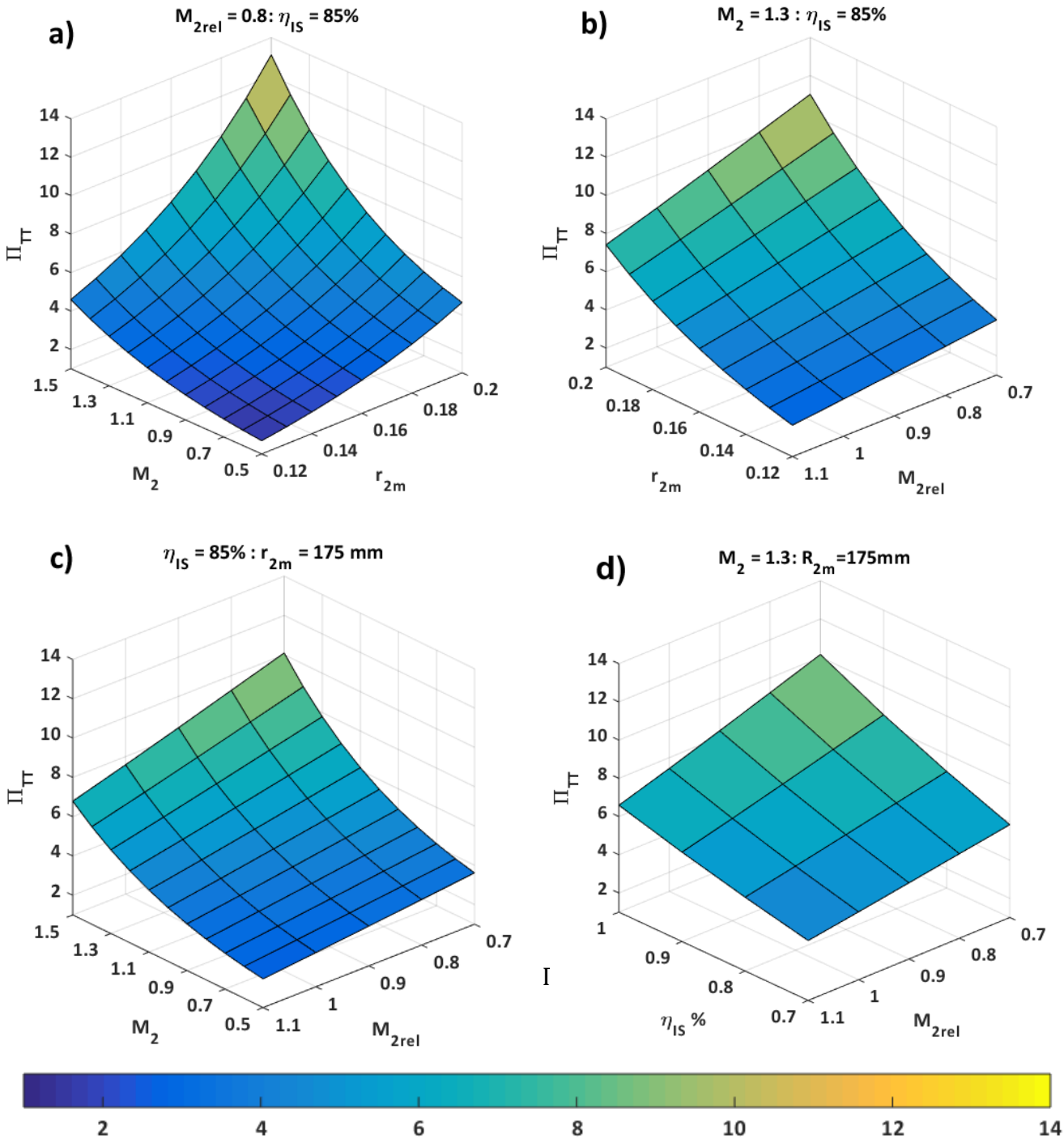


*Figure 13 (a-d) Rotor mean-line evaluation study plots*

The variation of exit flow angle ($\alpha_{2m}$) with respect to the axial direction is shown in ***Figure 14.*** Minimum $\alpha_{2m}$ is desired as it reduces the necessity of the stator to turn the flow back to axial direction. A lower $M_2$ corresponds to a higher $\alpha_{2m}$ and it is not beneficial for the cause as it generates lesser rotor pressure ratio. The minima for $\alpha_{2m}$ is in the $M_{2m}$ range of 1.1-1.3 with $\Pi_{TT}$ in 4.5-7 range. Higher $M_{2rel}$ gives a lower $\alpha_{2m}$ and correspondingly lower $\Pi_{TT}$. Blade exit angle ($\beta_{2m}$) variation with $M_{2m}$ is shown in ***Figure 15***. $\beta_{2m}$ constantly reduces with increasing $M_{2m}$. A lower $\beta_{2m}$ is beneficial as lesser turning in the rotor blade would avoid flow separation. An inflection point is observed at $M_{2m} = 1$ where higher subsonic diffusion in rotor relative frame requires lower $\beta_{2m}$ for $M_{2m}>1$ and vice versa for $M_{2m} < 1$. As concluded from the previous inferences higher diffusion in the rotor frame corresponds to increase in $\Pi_{TT}$.

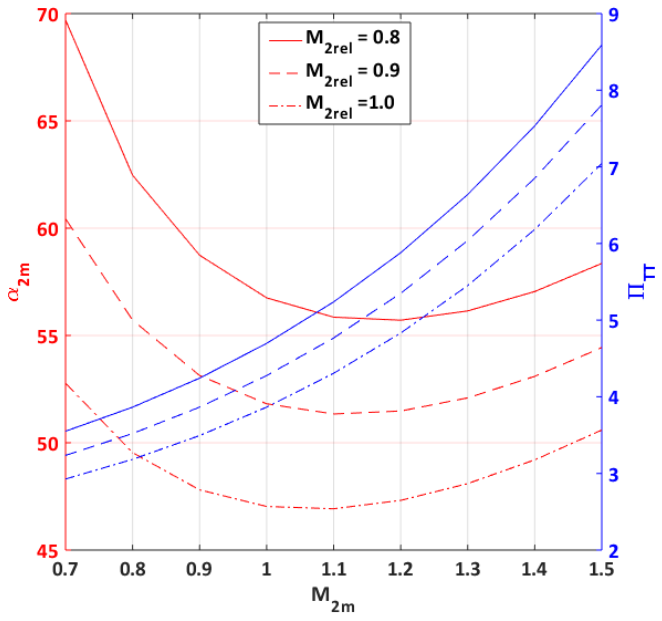


***Figure 14 Rotor flow exit angle variation with $M_2$***

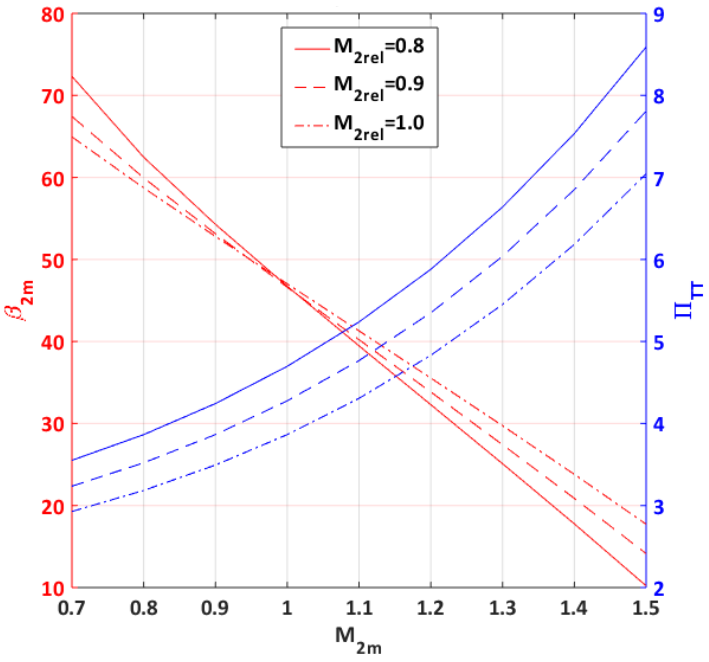


*Figure 15 Rotor blade exit angle variation with $M_2$*

The mean-line code predicts many of the rotor parameters to start with but a few more performance parameters need to be analyzed to gather a comprehensive knowledge of the mixed-flow rotor design process. Hence, we perform a computational analysis with a 3D RANS code to evaluate the rotor exit meridional angle, rotor axial length, number of blades and few other parameters which would provide the optimum rotor performance for the chosen design point. Details of this CFD analysis is given in a subsequent paper *Sadagopan and Camci* [2].

**Table 2 Mixed-flow rotor computational study cases**

| Case | $\Phi_2$ (degrees) | $L_R$ (mm) |
|---|---|---|
| a | 10 | 130 |
| b | 10 | 150 |
| c | 10 | 170 |
| d | 30 | 140 |
| e | 60 | 118 |
| f | 90 | 100 |

The rotor meridional angle study is conducted for a wide range of $\Phi_2$ from 0-90°. The same mean exit radius condition and Ω is maintained for cases (b, d, e and f) to understand the changes in pressure ratio, efficiency etc. It

is widely established that a centrifugal compressor generates high-pressure ratio compared to an axial design with some compromise on the efficiency. This study is primarily conducted to understand performance changes when a mixed-flow design is derived from a centrifugal rotor variant. The rotor geometrical variation is shown in ***Figure 16.*** Property value on the Y-axis corresponds to quantities mentioned in the legend.

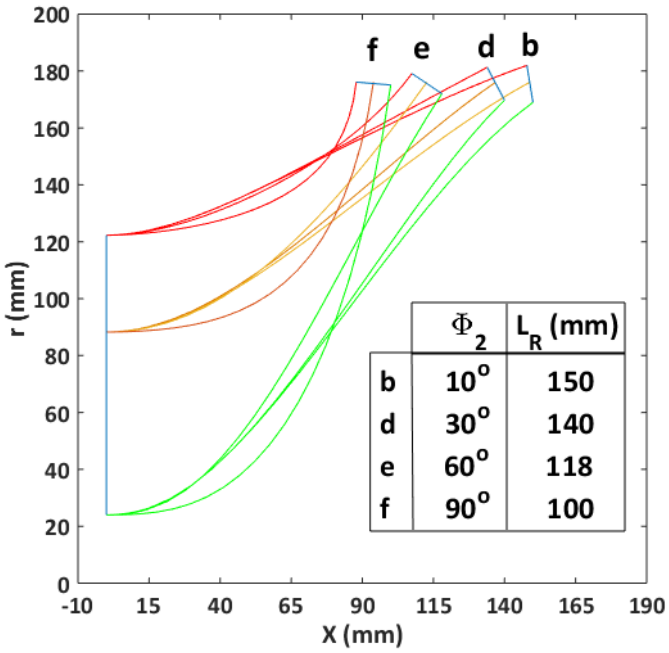


***Figure 16 Rotor meridional exit angle, $\Phi_2$ variation in meridional view with $\Phi_1 = 0^o$.***

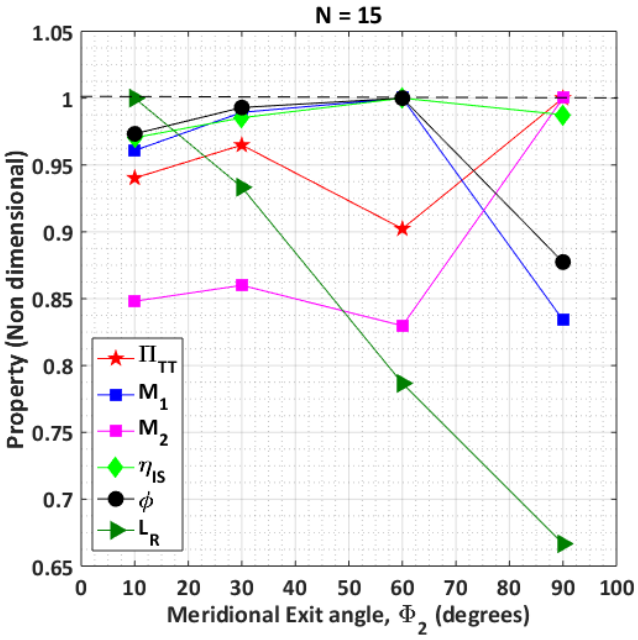


*Figure 17 Relative parametric analysis for meridional exit angle study*

The axial length of the rotor is increased with reduction in the $\Phi_{2m}$ angle to instill same amount of work into the fluid. Relative parametric variation in each of the configuration is shown in *Figure 17.* $\Pi_{TT}$ variation is within 10% margin for all the cases. Efficiency varies relatively in a 3% margin. The result shows that it is possible to derive a mixed-flow rotor from a centrifugal variant preserving the efficiency and pressure ratio. Increment in axial length for reducing $\Phi_{2m}$ value imparts extra work on the fluid when compared to a higher $\Phi_{2m}$ with lower axial length case. Additional axial length would add extra weight to the stage but a reduced $\Phi_{2m}$ would lead to a reduced frontal area of the engine, hence reduction in drag force. Pressure ratio and relative Mach number meridional contour plot in all the 4 cases are described in *Figure 18 and 19.*

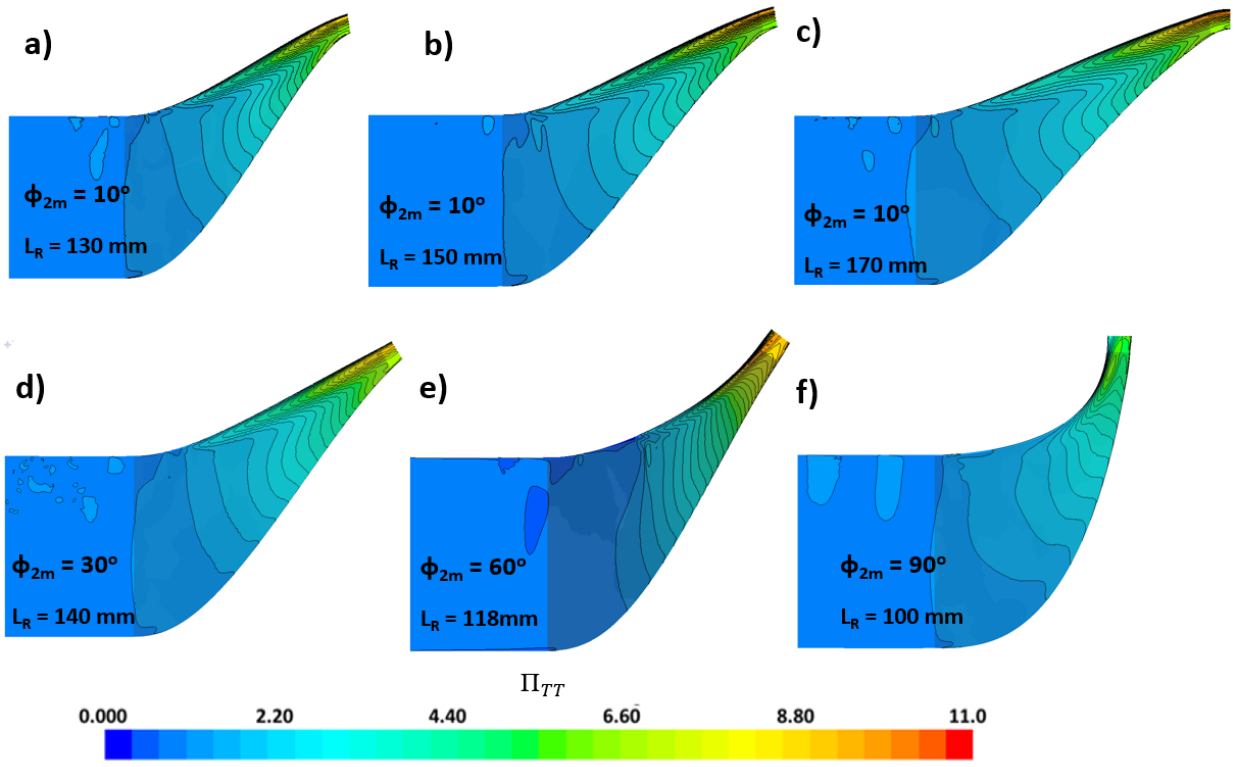


*Figure 18 Pressure ratio in the meridional view on 6 cases (a-f).*

A lower back pressure leads to a higher $M_2$ at exit as evident in *Figure 17*. Inlet Mach number $M_1$ and mass flow rate drops for the 90° case. Hub and casing contour play a very important role in pressure distribution throughout the passage. The low momentum zone is minimum for the 90° case which is shown in the form of maximum efficiency. Higher Pressure ratio growth is observed for cases with higher passage diffusion. This effect is dominantly observable near the casing surface. $\Phi_{2m}$ = 60° case has a smaller region of low momentum zone due to casing separation thus the diffusion is less compared to other cases. This effect is visible as the rotor pressure ratio is lower but efficiency is higher. $\Phi_{2m}$ = 60° and 90° tend to behave in a beneficial manner with regard to casing separation. To obtain the desired goal of minimum frontal area $\Phi_{2m}$ = 10° case is chosen. The conclusion matches the inference presented by *Eisenlohr and Benfer* [11] on mixed-flow rotor designs.

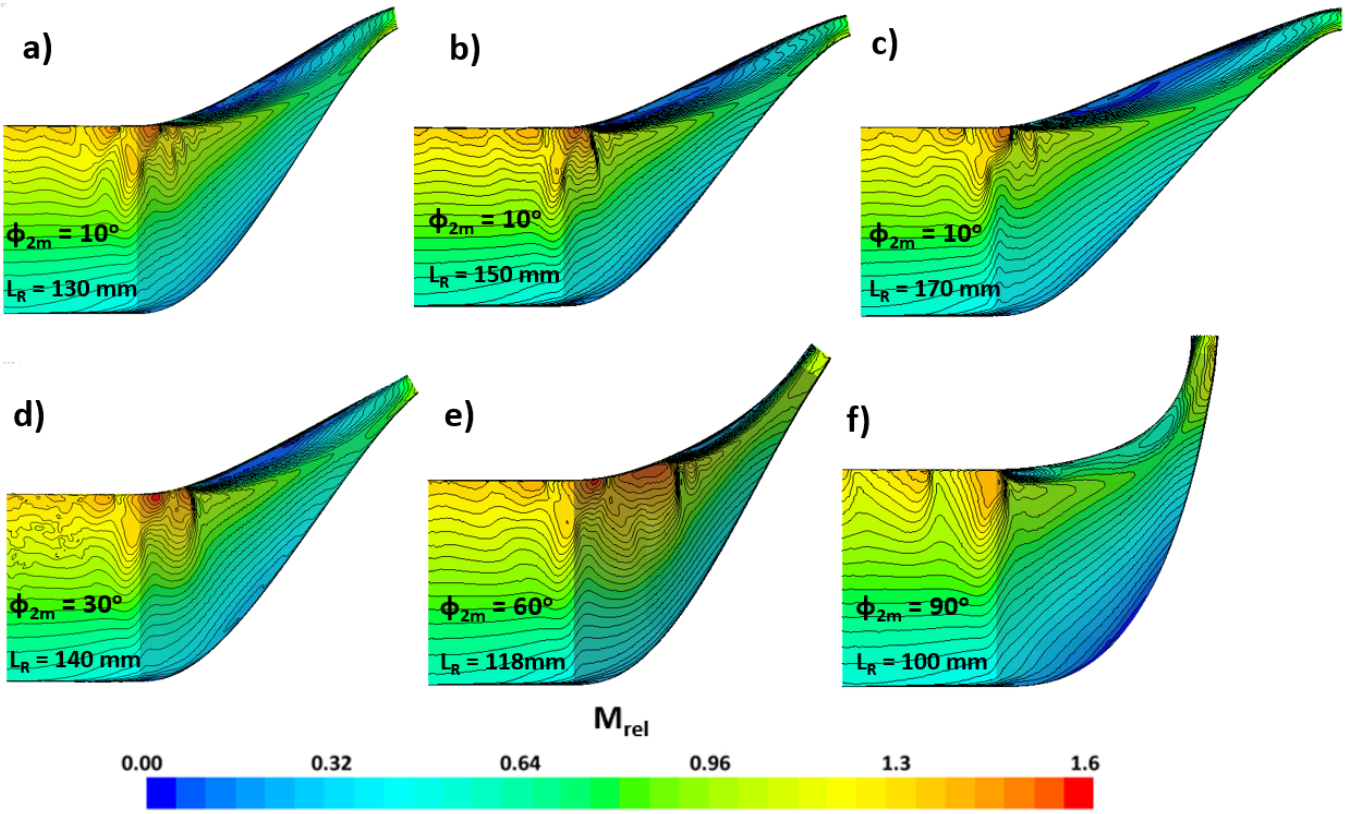


*Figure 19 Relative Mach no distribution for cases a-f in the meridional view*

A **rotor axial length ($L_R$) study** is conducted for 3 cases of a: 130mm, b: 150mm and c: 170mm as shown in *Figure 20*. $r_{2m}$, Ω and computational boundary conditions are same for all the 3 cases. *Figure 21* shows the non-dimensional parametric variation for the 18 bladed rotor design. It is clearly seen that $\Pi_{TT}$ increases with increasing $L_R$ as more blade surface performs more work on the fluid. Nearly a 9% increment in $\Pi_{TT}$ is observed in the 40mm $L_R$ increment. $M_2$ follows the same trend as $\Pi_{TT}$. Contrarily this increment in $\Pi_{TT}$ also adds blade weight. The main criteria for selection are rotor weight and $\eta_{IS}$. Rotor with 150 mm length shows maximum efficiency out of the 3 cases. 170mm case has relatively 4.5% decrement in efficiency due to higher viscous losses with the extended blade surface. Rothalpy losses consistently increase in the blade passage due to increment in length. 150 mm case is chosen for its weight and efficiency benefits. Pressure ratio and relative Mach number meridional contour plot of these 3 cases are described in *Figure 18 and 19*.

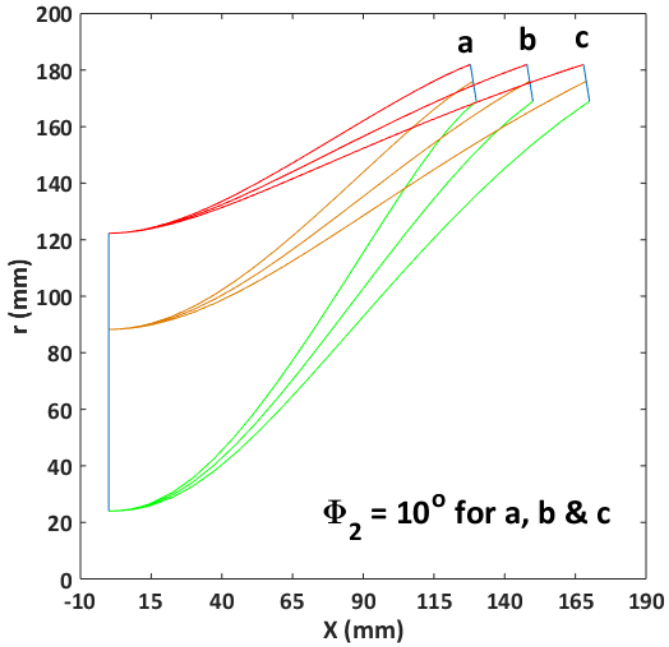


*Figure 20 Rotor axial length, LR variation in meridional view where a: $L_R$ = 130mm, b: $L_R$ = 150mm, c: $L_R$ = 170mm with $\Phi_2$ = 10° and $\Phi_1$ = 0°.*

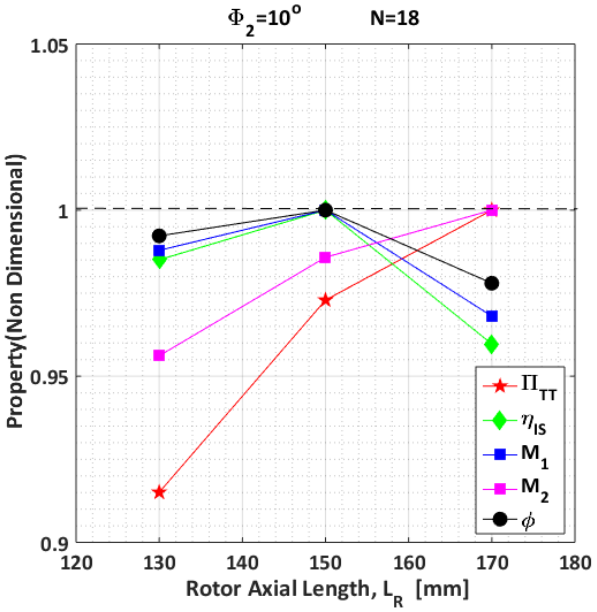


*Figure 21 Relative parametric study for rotor axial length variation*

A brief discussion on the **rotor blade loading** along span is provided based on *Xuanyu et al* [16]. For the hub line near the leading edge, centrifugal force cannot generate high-pressure ratio as the meridional passage height is not increasing abruptly. The hub line height increases in the posterior side so any loading increment in this zone will

enhance pressure rising capability. Higher loading in the hub frontal area provided with over bending of the blade will lead to flow separation on the suction side causing reduction in efficiency. Conversely for the tip region higher loading near the frontal area will increase rotor's pressure rising ability and a decreased loading in the tip posterior area will help in controlling the inevitable suction side separation of tip region. Conclusively, increasing hub loading makes impeller achieve higher performance with lower tip leakage loss and uniform flow outlet at exit. Increasing tip loading makes the impeller achieve high-pressure ratio.

**Rotor pitch variation study** is conducted by varying the number of blades on the hub surface shown in *Figure 22*. 18 bladed configuration imparts highest energy into the fluid as evident from the $M_2$ and $\Pi_{TT}$ values. All the parameters vary in a very narrow margin of 5-6%. Rotor mass consistently increases by relative 1.6% for each additional blade. A 10 bladed configuration would deliver a 5% decrement in performance for 16% reduction in weight.

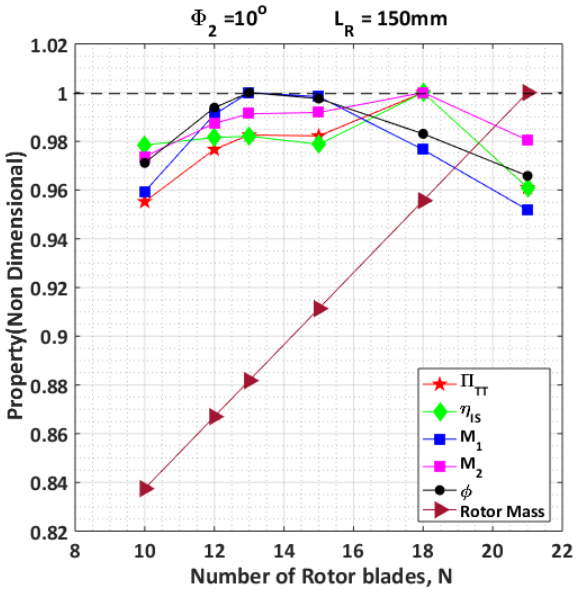


*Figure 22 Relative parametric variation for rotor pitch variation study*

Based on findings of *RajaKumar et al* [18], for a mixed-flow rotor with subsonic rotor passage flow the **tip leakage flow** interacts with the main passage flow contributing significantly to the losses. Choke mass flow increases with higher inlet area due to increment in tip clearance. Surge occurs earlier due to separation tendency exhibited by interaction of the cross flow with main flow in the clearance space. Pressure ratio and performance drops linearly compared to impeller shroud gap. Pressure drop at the tip section is more due to the leakage and main flow interaction.

Mid plane blade loading has no impact of tip clearance variation. Static pressure rise across the rotor passage reduces with increasing tip clearance. A constant tip clearance performs better than a variable tip clearance based on *Rammamurthy et al* [17]. They also conclude that a classical jet wake flow observable in a centrifugal rotor is absent for a mixed-flow rotor. Mixed and centrifugal impellers have similar flow structures, but the mixed-flow design performs better than centrifugal due to lower tip leakage loss with a more uniform flow field at rotor outlet according to *Xuanyu et al.* [16]. In this effort, all of the designed rotors had a constant tip clearance of 1mm. Tip leakage occurring from pressure to suction side in the initial tip section leading edge merged with casing separated low momentum fluid. In the mid chord section, certain streamlines travelled all the way from the pressure side hub region to suction side tip region through the gap, eventually mixing with the low momentum fluid.

# VII. Conclusions

The main objective of this paper is to provide a strategic design guidance for a single-stage mixed-flow compressor with high-pressure ratio of 6:1 in the (1-10) $kg.s^{-1}$ mass flow range. A brief historical background of the previous designs including pros and cons of this design compared to centrifugal and axial stages in the small engine segment is presented. As noted, most of the earlier designs suffered from inefficient stator performance which could not accommodate the high blade loading requirement. In the next few decades supersonic tandem stator designs had been attempted to distribute the high blade loading but none of them could provide an efficiency above 80 %.

A simple mean-line mixed-flow stage design procedure has been provided based on the first principles. As it does not involve any empirical formulas to predict losses it could be used as an initiating point for designers to comprehensively grasp the fundamentals of mixed-flow type turbomachinery design. With the definition of geometric parameters, this step is furthered by the geometry design technique based on Bezier curves. For the stator, we generate a 2D cascade design for the tandem configuration which is further developed into 3D based on hub and casing definitions.

Then, the rotor design is evaluated based on the mean-line equations which concludes that a high-pressure ratio inadvertently demands the requirement for a supersonic rotor exit flow with high flow exit angle in the range of 47-60$^o$ from the axial direction. Efficiency values increase with high rotor passage diffusion. A higher rotor exit Mach number, higher exit mean radius and low rotor exit relative Mach number is desired to obtain a high-pressure ratio. To obtain an increment in isentropic efficiency for the same pressure ratio, $M_2$ should reduce and $M_{2rel}$ should increase. Optimum $\alpha_{2m}$ is in the $M_{2m}$ range of 1.1-1.3 generating rotor $\Pi_{TT}$ up to 4.5-7. Higher $M_{2rel}$ gives a lower $\alpha_{2m}$ and correspondingly lower $\Pi_{TT}$. In the blade exit angle $\beta_{2m}$, an inflection point is observed at $M_{2m} = 1$ where higher subsonic diffusion in rotor relative frame requires lower $\beta_{2m}$ for $M_{2m}>1$ and vice versa for $M_{2m} < 1$.

Though most of the design parameters could be analyzed in the 1D system, few other crucial parameters like rotor meridional exit angle, axial length, blade solidity, blade loading and tip leakage are comprehended using multidimensional and viscous computational analysis. Higher hub loading makes impeller achieve higher performance with lower tip leakage loss and uniform flow outlet at exit. Increasing tip loading makes the impeller

achieve high-pressure ratio. The results show that it is possible to derive a mixed-flow rotor from a centrifugal variant reasonably preserving the efficiency and pressure ratio.

The challenging objective of supersonic diffusion and high flow turning with high efficiency and stagnation pressure recovery is achieved with a tandem stator design based on *Quishi et al* [1]. Acceleration of low momentum flow zones of the first blade by suction side of the second blade increases diffusion efficiency. This tandem stator design provides significant performance benefits when compared with the previous mixed-flow stage designs. The design strategy for supersonic tandem diffuser explained in this paper is straight forward to implement in a modern single-stage mixed-flow compressor design effort.

Conclusively, a mixed-flow stage design with pressure ratio 5.83 and 75.5% efficiency is evident from this effort as observed and quantified from the computational RANS simulations. A pressure ratio of 6.12 is also achievable with only a 3.5% rotational speed increase, at $\Omega/\Omega_o = 1.035$. The current approach presents a complete mixed-flow compressor design system. The method results in relatively high-performance compressors when compared to existing mixed-flow type designs in open literature. They are much shorter than corresponding axial designs with additional system weight and maintenance benefits. The detailed multi-dimensional and viscous/compressible stage simulations including shock wave influence to obtain more realistic performance parameters are topic of a subsequent paper by *Sadagopan and Camci* [2].

## Conflict of interest statement

The authors certify that they have NO affiliations with or involvement in any organization or entity with any financial interest (such as honoraria; educational grants; participation in speakers' bureaus; membership, employment, consultancies, stock owner- ship, or other equity interest; and expert testimony or patent- licensing arrangements), or non-financial interest (such as personal or professional relationships, affiliations, knowledge or beliefs) in the subject matter or materials discussed in this manuscript.

## Acknowledgments

The authors wish to thank Dept.of Aerospace Engineering for the assistantship provided to Mr.Aravinth Sadagopan. Kirk Heller, Benjamin Enders and Mark Catalano's support was invaluable for maintaining the high-performance computing infrastructure involved in the current effort.

## VIII. References

[1] Quishi, L., Hong, W., Sheng, Z., 2009," Application of tandem cascade for fan stator with supersonic inflow", Chinese Journal of Aeronautics 23(2010) 9-14. https://doi.org/10.1016/S1000-9361(09)60181-3 .

[2] Sadagopan, A., Camci, C., 2018," Viscous flow analysis and performance predictions of a 6:1 supersonic mixed flow compressor with a tandem diffuser", Aerospace Science and Technology, Elsevier, under review.

[3] King, J.A. and Glodeck, E., 1942, "Performance characteristics of mixed-flow impeller and vaned diffuser with several modifications," NACA MR E197.

[4] Laskin, E.B. and Kofskey, M.G., 1947, "Performance of a mixed-flow impeller in combination with a semivaneless diffuser" NACA RM E7C05a.

[5] Brown, W.B. and Bradshaw G. R., 1947,"Design and Performance of family of diffusing scrolls with mixed-flow impeller and vaneless diffuser", NACA Report 936.

[6] Wilcox, W.W. and Robbins W. H., 1951,"Design and performance of an experimental axial discharge mixed-flow compressor", NACA RM E51A02.

[7] Hamrick, J.T. and Osborn W. M., 1955,"Design and test of mixed-flow impellers V-Design procedure and performance results for two vaned diffusers with impeller model MFI – 1B", NACA RM E55E13.

[8] Dallenbach, F., 1961,"The aerodynamic design and performance of centrifugal and mixed-flow compressors", SAE International Congress and Exposition of Automotive Engineering, Detroit, MI, January 9-13, 1961, SAE 268A.

[9] Dodge, J.L., Bush, D.B., Pechuzal, G.A. and Ravindranath, A., 1987," High efficiency transonic mixed-flow compressor method and apparatus", U.S. Patent 4,678,398.

[10] Musgrave, D. S. and Plehn, N.J., 1987,"Mixed-flow compressor stage design and test results with a pressure ratio of 3:1", ASME J. Turbo., Vol. 109/513. https://doi.org/10.1115/1.3262141.

[11] Eisenlohr, G. and Benfer, F.W., 1993,"Aerodynamic design and investigation of a mixed-flow compressor stage", Presented at AGARD Meeting "Technology Requirements for Small Gas Turbines", 8 p (SEE N94-34431 10-07).

[12] Elmendorf, W., Kurz, H., Gallus, H.E., 1995,"Design and experimental investigation of a mixed-flow supersonic compressor stage", Presented at the International Gas Turbine and Aero-engine Congress and exposition, Houston, TX, June 5-8, 1995, 95-GT-379. https://doi.org/10.1115/95-GT-379.

[13] Youssef, N. and Weir, G., 2002,"Mixed-flow and centrifugal compressor for gas turbine engine", U.S. Patent 6,488,469 B1.

[14] Hazby, H., Casey, M., Numakura, R. and Tamaki, H., 2015,"A transonic mixed-flow compressor for an extreme duty", ASME J. Turbo. May 2015, Vol. 137/051010. https://doi.org/10.1115/GT2014-25378.

[15] Giri, G., Nassar, A., Moroz, L., Klimov, I.V., Sherbina, A., 2016,"Design and analysis of a high-pressure ratio mixed-flow compressor stage", AIAA Propulsion and Energy forum, July 25-27, 2016, Salt Lake City, UT, AIAA 2016-4744. https://doi.org/10.2514/6.2016-4744.

[16] Xuanyu, C., Xiangwei, M., Xingmin, G. and Donghai, J., 2014,"The aerodynamic design and investigation of loading distribution of a mixed-flow compressor", APISAT2014, Procedia Engineering 99(2015) 484-490. https://doi.org/10.1016/j.proeng.2014.12.562 .

[17] Ramamurthy, S., Srharsha, A. M., 2009, 'Theoretical evaluation of flow through a mixed flow compressor stage' in 19th International Symposium on Air Breathing Engines, Proceedings of the ISABE.

[18] Rajakumar, R. D., Ramamurthy, S., Govardhan, M., 2013,"Study on the performance deterioration of mixed-flow impeller due to change in tip clearance", Journal of Thermal Science, Vol.22, No.6. DOI: 10.1007/s11630-013-0659-1 .

[19] Cevik, M., Uzol, O., Yavrucuk, I., 2009, "A robust design optimization of a mixed-flow compressor impeller", ASME. Turbo Expo: Power for Land, Sea, and Air, Volume 7: Turbomachinery, Parts A and B, 699-707. https://doi.org/10.1115/GT2009-60298 .

[20] Monig, R., Elmendorf, W., Gallus, H. E., 1993, 'Design and Rotor Performance of a 5:1 Mixed-flow Supersonic Compressor', ASME J. Turbo, July 1993, Vol. 115 (3), pp 565-572, doi: 10:1115/1.292929.

[21] Hill, P., and Peterson, C., 1992, Mechanics and Thermodynamics of Propulsion, 2nd Ed.Addison-Wesley Publishing company, Inc. ISBN-13: 978-0201146592 .

[22] Japikse, D. and Baines, N. C, 2000, Diffuser Design Technology, White River Junction, VT: Concepts ETI, Inc, 1998. ISBN-13: 978-0933283084 .

[23] Merchant, A., Kerrebrock, J. L., Adamcyzk, J. J., Braunscheidel, E., 2005,'Experimental Investigation of a High Pressure Ratio Aspirated Fan stage', ASME J Turbo., January 2005, Vol. 127/43. https://doi.org/10.1115/1.1812323 .